Two Rings of Negative Charges in the Cytosolic Vestibule of Type-1 Ryanodine Receptor Modulate Ion Fluxes

Le Xu,* Ying Wang,* Dirk Gillespie,† and Gerhard Meissner*
*Department of Biochemistry and Biophysics, University of North Carolina, Chapel Hill, North Carolina 27599; and †Department of Molecular Biophysics and Physiology, Rush University Medical Center, Chicago, Illinois 60612

ABSTRACT The tetrameric ryanodine receptor calcium release channels (RyRs) are cation-selective channels that have pore architecture similar to that of K^+ channels. We recently identified, in close proximity to the selectivity filter motif GGGIG, a conserved lumenal DE motif that has a critical role in RyR ion permeation and selectivity. Here, we substituted three aspartate residues (D^{4938}, D^{4945}, D^{4953}) with asparagine and four glutamate residues (E^{4942}, E^{4948}, E^{4952}, E^{4955}) with glutamine hypothesized to line the cytosolic vestibule of the skeletal muscle RyR (RyR1). Mutant single channel properties were determined using the planar lipid bilayer method. Two mutants ($D^{4938}N$, $D^{4945}N$) showed a reduced K^+ ion conductance, with $D^{4938}N$ also exhibiting a reduced selectivity for Ca^{2+} compared to K^+. The cytosolic location of D^{4938} and D^{4945} was confirmed using the polycation neomycin. Both $D^{4938}N$ and $D^{4945}N$ exhibited an attenuated block by neomycin to a greater extent from the cytosolic than lumenal side. By comparison, charge neutralization of lumenal loop residues ($D^{4899}Q$, $E^{4900}N$) eliminated the block from the lumenal but not the cytosolic side. The results suggest that, in addition to negatively charged residues on the lumenal side, rings of four negative charges formed by D^{4938} and D^{4945} in the cytosolic vestibule determine RyR ion fluxes.

INTRODUCTION

Ryanodine receptor ion channels (RyRs) regulate various cellular functions by releasing Ca^{2+} from intracellular Ca^{2+} stores (1–3). The RyRs are cation-selective channels that have a high ion conductance for both monovalent (~800 pS with 250 mM K^+ as conducting ion) and divalent (~150 pS with 50 mM Ca^{2+}) cations, yet do so selectively ($P_{Ca}/P_K \sim 7$) (4–6). Since RyR is highly cation selective, it is likely that negative charges line the pore of this channel. The location of these charges in RyR has been probed using large organic and inorganic positively charged molecules. Monovalent cations produced well-resolved voltage-dependent blocking events from the cytosolic side (7,8), whereas polycations such as neomycin or ruthenium red were capable of blocking RyR channels from both sides (9–12). These studies indicated the presence of negatively charged residues on both the cytosolic and lumenal ends of the conductance pathway of the RyRs.

Mammalian RyRs have ~70% sequence identity, with the highest level of identity in the C-terminal, pore-forming region. Hydropathy analysis initially suggested between 4 and 12 transmembrane segments per RyR subunit (13,14). More recent studies have indicated the presence of six to eight transmembrane helices in each RyR1 subunit (15). The most C-terminal membrane-spanning segment of RyR has been proposed to be the inner helix of the pore (16), and amino acid residues linking the two C-terminal membrane-spanning segments are believed to correspond to the pore-forming segment of K^+ channels. Sequence comparison and mutagenesis studies have also suggested that the RyR ion channels have a pore structure similar to that of K^+ channels (whose structure is known) (17–22). In RyR, the residues between the two C-terminal membrane-spanning segments are lumenally located (23) and have a predicted pore helix followed by an amino acid motif (GGGIG) that is similar to the selectivity filter motif (TV/IGYG) of K^+ channels (24).

However, there exist significant functional and sequence differences. First, K^+ channels selectively conduct K^+ ions, whereas RyRs have a high ion conductance for both monovalent and divalent cations. Second, the RyR pore has a minimum radius of ~3.5 Å as estimated from the relative permeability of organic cations (25), compared to a radius of ~2 Å for K^+ channels (26). Third, mutagenesis and single channel measurements have shown that a conserved RyR lumenal DE motif in close proximity to the selectivity filter motif GGGIG has a critical role in RyR ion permeation and selectivity (21); the two amino acids are not fully conserved or even absent in K^+ channels.

In this study, we mutated seven negatively charged amino acid residues hypothesized to line the cytosolic vestibule of RyR1. Charge neutralization of two acidic residues (D^{4938} and D^{4945}) closely following the most C-terminal membrane-spanning segment reduced RyR1 K^+ ion permeation, with $D^{4938}N$ also exhibiting a reduced Ca^{2+} selectivity. The cytosolic location of these two residues was confirmed using the polycationic RyR blocker neomycin. Substitution of D^{4938} or D^{4945} with asparagine attenuated block by neomycin to a greater extent from the cytosolic than lumenal side. The results suggest that, in addition to negatively charged residues on the lumenal side, rings of negative

Submitted August 11, 2005, and accepted for publication October 4, 2005.

Le Xu and Ying Wang contributed equally to this work.

Address reprint requests to Gerhard Meissner, Tel.: 1-919-966-5021; Fax: 1-919-966-2852; E-mail: meissner@med.unc.edu.

0006-3495/06/01/443/11 $2.00

doi: 10.1529/biophysj.105.072538

charges in the cytosolic vestibule have a role in maintaining the high RyR1 ion fluxes.

EXPERIMENTAL PROCEDURES

Materials

Human embryonic kidney (HEK) 293 cells were obtained from ATCC, [^{3}H]ryanodine from Perkin Elmer Life Sciences (Boston, MA), unlabeled ryanodine from Calbiochem (La Jolla, CA), Fluo-4-AM from Molecular Probes (Eugene, OR), complete protease inhibitors from Roche (Indianapolis, IN), and phospholipids from Avanti Polar Lipids (Alabaster, AL). All other chemicals were of analytical grade.

Construction of mutant cDNAs

For construction of RyR1 mutants, a fragment (*Cla1*/*Xba1,14443*/*15276*) of the full length rabbit RyR1 cDNA subcloned into pBluescript vector (20) was used as template for mutagenesis. Single base changes were introduced by *Pfu*-turbo polymerase-based chain reaction using mutagenic oligonucleotides and the QuikChange site-directed mutagenesis kit (Stratagene, La Jolla, CA). The complete mutated sequences were confirmed by DNA sequencing and subcloned back into the *Cla1* and *Xba1* sites of pCMV5 vector containing *EcoR1*/*Xba1* fragment of RyR1. Mutated full-length expression plasmids were prepared by ligation of three fragments (*Cla1*/*Xho1*, *Xho1*/*EcoR1, EcoR1*/*Xba1* containing the mutated sequence) and expression vector pCMV5 (*Cla1*/*Xba1*) as described (20). Nucleotide and amino acid numbering are as described (13).

Expression of full-length wild-type and mutant RyRs in HEK 293 cells

RyR1 cDNAs were transiently expressed in HEK 293 cells using FuGENE 6 (Roche Applied Science) as described (21). Crude membrane fractions and proteoliposomes containing the purified 30 S wild-type and mutant RyR1 ion channels were prepared in presence of protease inhibitors (21).

Ca^{2+} release measurements

Cellular Ca^{2+} release in response to caffeine was determined with the fluorescence Ca^{2+} indicator dye Fluo-4 (21). HEK 293 cells transfected with cDNA encoding wild-type or mutant RyR1s were grown for 48 h on glass coverslips and, after washing with phosphate-buffered saline, were loaded with 5 μM Fluo-4-AM for 1 h at 37°C in Krebs-Ringer-Henseleit (KRH) buffer (125 mM NaCl, 5 mM KCl, 1.2 mM KH_2PO_4, 6 mM glucose, 1.2 mM $MgCl_2$, 2 mM $CaCl_2$, and 25 mM HEPES, pH 7.4). After rinsing with KRH buffer to remove nonhydrolyzed fluorophore, cells were transferred to a recording chamber with KRH buffer and Fluo-4 fluorescence was recorded and analyzed using a Photon Technology International Deltascan system attached to an inverted microscope (TE 300; Nikon) and ImageMaster program (Photon Technology International, Lawrenceville, NJ). Caffeine responsiveness of cells was recorded by rapid addition of freshly made caffeine solution to a final concentration of 10 mM.

[^{3}H]Ryanodine binding

Ryanodine is a widely used probe of channel activity because of its preferential binding to the open channel state (2,27). B_{max} values of [^{3}H]ryanodine binding were determined by incubating membranes for 4 h at 24°C with a saturating concentration of [^{3}H]ryanodine (40 nM) in 20 mM imidazole, pH 7.0, 0.6 M KCl, 0.15 M sucrose, 5 mM oxidized glutathione, 20 μM leupeptin, 200 μM Pefabloc, and 100 μM Ca^{2+}. To determine Ca^{2+} dependence of [^{3}H]ryanodine binding, membranes were incubated for 20 h at 24°C with 2.5 nM [^{3}H]ryanodine in 20 mM imidazole (pH 7.0), 0.15 M sucrose, 250 mM KCl, protease inhibitors, 5 mM oxidized glutathione, and free Ca^{2+} concentrations ranging 0.5–500 μM. Samples were diluted with eight volumes of ice-cold water and placed on Whatman (Brentford, UK) GF/B filters preincubated with 2% polyethyleneimine in water. Filters were washed with three 5 ml aliquots of ice-cold 100 mM KCl, 1 mM KPipes (pH 7.0) solution. The radioactivity remaining with the filters was determined by liquid scintillation counting to obtain bound [^{3}H]ryanodine. Nonspecific binding was determined using a 1000–2000-fold excess of unlabeled ryanodine.

Single channel recordings

Single channel measurements were performed using Mueller-Rudin type planar lipid bilayers containing a 5:3:2 mixture of bovine brain phosphatidylethanolamine, phosphatidylserine, and phosphatidylcholine (25 mg of total phospholipid/ml *n*-decane) (28). Proteoliposomes containing the purified RyRs were added to the *cis* (sarcoplasmic reticulum (SR) cytosolic side) chamber of a bilayer apparatus and fused in the presence of an osmotic gradient (250 mM *cis* KCl/20 mM *trans* KCl in 20 mM KHepes, pH 7.4, with 2–20 μM Ca^{2+} and 1 mM ATP in the *cis* chamber). After appearance of channel activity, *trans* (SR lumenal side) KCl concentration was increased to 250 mM to prevent further fusion of proteoliposomes. The *trans* side of the bilayer was defined as ground. The large cytosolic regulatory region of the channels faced the *cis* chamber in a majority (>98%) of the recordings (28). Electrical signals were filtered at 2 kHz (0.5 kHz for Ca^{2+} currents at 0 mV), digitized at 10 kHz, and analyzed as described (12).

To determine permeability ratios, single channel activities were recorded in symmetrical 250 mM KCl solution with 10 mM Ca^{2+} on the *trans* side and the reversal potential (E_{rev}) was measured. The permeability ratio of Ca^{2+}/K^+ ions (P_{Ca}/P_K) was calculated using a modified form of the Goldman–Hodgkin-Katz equation:

$$E_{rev} = -\frac{RT}{F} Ln\left\{ [K]^{\frac{1}{2}} \times \left([K] + 4\frac{P_{Ca}}{P_K}[Ca] \right)^{-\frac{1}{2}} \right\}, \quad (1)$$

where [Ca] is the concentration of Ca^{2+} ions on the *trans* side, and [K] is the concentration of K^+ ions on the *cis* and *trans* side.

Kinetic analysis of neomycin-induced partial block in ryanodine-modified channels

Cytosolic neomycin caused a substate at positive but not negative holding potentials, and lumenal neomycin caused a substate at negative but not positive holding potentials in ryanodine-modified RyR2 (11). The same results were obtained for ryanodine-modified wild-type and mutant RyR1s (see Figs. 3–5, *C* and *D*). The subconductance was analyzed by a simple biomolecular scheme (11).

For ryanodine-modified channels the closed events were rare. The occurrence of substates could therefore be assessed by the open probability (P_o), which was determined by 50% threshold analysis with cursors set on the ryanodine-modified state (see Figs. 3–5, *O*) and substate (see Figs. 3–5, *s*–):

$$P_s = 1 - P_o = 1/\{1 + K_{50}/[\text{neomycin}]\}, \quad (2)$$

where K_{50} is the concentration of neomycin at which P_s was 0.5. This approach also yields dwell times of modified state (T_o) and substate (T_s)

$$k_{on} = 1/T_o \quad (3)$$

$$k_{off} = 1/T_s \quad (4)$$

$$K_D = (k_{off}/k_{on})[\text{neomycin}], \quad (5)$$

where k_{on} and k_{off} are association and dissociation rate constants of neomycin and K_D is the dissociation constant. The relationships between K_D and holding potential were fitted using the following equation:

$$K_D(V) = K_D(0)\exp[-z_{total}(FV/RT)], \quad (6)$$

where z_{total} is the total effective gating charge of block induced by neomycin, F is the Farady constant, and V is holding potential.

Biochemical assays and data analysis

Free Ca^{2+} concentrations were obtained by including in the solutions the appropriate amounts of Ca^{2+} and EGTA as determined using the stability constants and the computer program published by Schoenmakers et al. (29). Free Ca^{2+} concentrations were verified with the use of a Ca^{2+}-selective electrode.

Results are given as mean ± SE. Significance of differences in the data ($p < 0.05$) was determined using Student's t-test.

RESULTS

The amino acid sequences of the predicted pore-forming regions of the skeletal muscle (type 1) ryanodine receptor are shown in Fig. 1. Shown are the lumenal loop linking the two most C-terminal transmembrane-spanning helices (*A*) and the most C-terminal transmembrane-spanning segment (C-terminal TM) and an extension by 22 amino acid residues (*B*). The lumenal loop has an amino acid motif (GGGIG) similar to the sequence TVGYG that determines the selectivity of the bacterial K^+ channel KcsA (24). In a recent study, we mutated the conserved glutamate and aspartate residues of the lumenal loop to asparagine and glutamine residues (indicated in *bold* in Fig. 1 *A*). We found that neutralizing the charge of two lumenal RyR1 residues (D^{4899}, E^{4900}) immediately after the GGGIG motif reduced K^+ ion conductance and selectivity for Ca^{2+} compared to K^+ (21). Here we consider whether neutralization of negative charges following the sequence of predicted C-terminal TM (indicated in *bold* in Fig. 1 *B*) would have similar effects.

We substituted three aspartate residues (D^{4938}, D^{4945}, D^{4953}) with asparagine and four glutamate residues (E^{4942}, E^{4948}, E^{4952}, E^{4955}) with glutamine. The mutants were expressed in HEK 293 cells, and their expression levels and functional properties were assessed by immunoblot analysis, cellular Ca^{2+} release, and [^{3}H]ryanodine binding, as previously described (21). Single channel recordings were performed to determine the ion permeation properties of the mutants.

Functional properties of RyR1 pore mutants

Immunoblot analysis showed that the seven RyR1 mutants were expressed in HEK 293 cells at a level comparable to wild-type (Fig. 1S, Supplemental Data). The ability of the mutants to release Ca^{2+} in response to the Ca^{2+}-releasing drug caffeine was determined in a cellular fluorescence assay using Fluo-4. Fig. 2 shows three representative Ca^{2+} release curves for vector-, wild-type-RyR1-, and RyR1-D^{4938}N-transfected cells. Vector-transfected cells showed no caffeine response, indicating that HEK 293 cells express endogenous RyRs at background levels. Similar time courses and peak amplitudes of Ca^{2+} release were observed for wild-type and RyR1-D^{4938}N (Fig. 2), as well as for RyR1-D^{4945}N, -E^{4948}Q, -E^{4952}Q, and -E^{4955}Q (Fig. 2S, Supplemental Data, Table 1). Two mutants (RyR1-E^{4942}Q and -D^{4953}N) displayed a background signal comparable to vector-transfected cells (Table 1).

The expression of functional RyR1 mutant proteins was also probed by determining their ability to bind [^{3}H]ryanodine (2,27). Four of the seven mutants (RyR1-D^{4938}N, -D^{4945}N, -E^{4952}Q, -E^{4955}Q) bound [^{3}H]ryanodine (Table 1) and showed Ca^{2+} dependence of [^{3}H]ryanodine binding close to that of wild-type RyR1 (Fig. 3S, Supplemental Data). The two mutants (E^{4942}Q and D^{4953}N) that failed to show a caffeine response also exhibited a loss of high-affinity [^{3}H]ryanodine binding. RyR1-E^{4948}Q exhibited a caffeine response but showed greatly reduced levels of [^{3}H]ryanodine

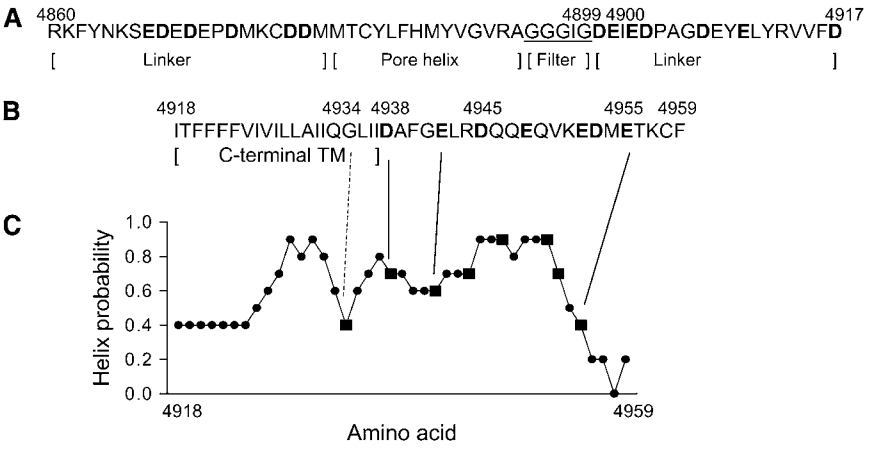

FIGURE 1 Pore-lining sequences of RyR1. Shown are the amino acid sequences of lumenal loop spanning the two most C-terminal transmembrane-spanning segments (*A*) and the most C-terminal transmembrane-spanning segment (C-terminal TM) and an extension by 22 residues (*B*). C-terminal TM corresponds to TM4 of the four membrane-spanning model of Takeshima et al. (13) and TM10 (without N-terminal amino acid residues VVFD) of the 12 membrane-spanning model of Zorzato et al. (14) used by Du et al. (15) to describe an 8 membrane-spanning model. (*C*) Helical probability of putative C-terminal TM and 22 residues immediately after C-terminal TM was calculated, using the PROF protein sequence analysis program (42,43). In *A*, the putative RyR1 pore helix, selectivity filter, and linker regions are shown. Bold indicates negatively charged amino acid residues mutagenized to asparagine or glutamine (21, this study). Underlined amino acids indicate residues analogous to the selectivity filter of K^+ channels (26).

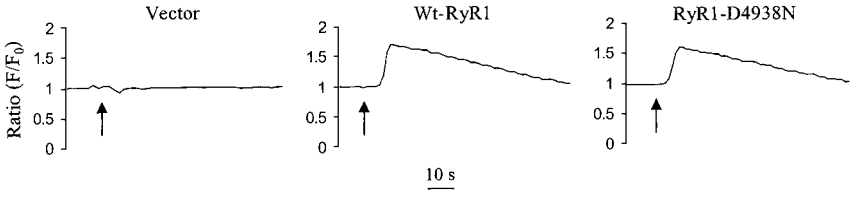

FIGURE 2 Caffeine-induced Ca^{2+} release in HEK 293 cells expressing wild-type RyR1 and RyR1-$D^{4938}N$. HEK 293 cells were transfected with pCMV5 vector, wild-type RyR1 and RyR1-$D^{4938}N$ cDNAs. The fluorescence intensity of Fluo-4 loaded cells was measured before and after addition of 10 mM caffeine. Arrows indicate the addition of caffeine. Representative traces are shown.

binding (Table 1), which indicated loss of function during membrane isolation.

K^+ conductance of RyR1 mutant channels

The ion permeation properties of the mutant RyR1 ion channels that showed retention of function were determined by fusing proteoliposomes containing the purified 30 S channel complexes with planar lipid bilayers. Single channels were recorded in 250 mM KCl medium on both sides of the lipid bilayer with K^+ as current carrier. Single channel currents can be efficiently recorded in KCl solutions because RyR does not noticeably conduct anions like Cl^- and conducts monovalent cations more efficiently than Ca^{2+}. The *cis* (cytosolic) bilayer chamber contained micromolar activating Ca^{2+} (2–20 μM) and 1 mM ATP to increase single channel activity. To ascertain retention of pharmacological regulation, cytosolic Ca^{2+} concentrations were reduced to 0.1 μM and increased to 100 μM. We found that the mutants that retained both caffeine response and [^{3}H]ryanodine binding exhibited a Ca^{2+} dependence similar to that of wild-type RyR1 (Fig. 4S, Supplemental Data).

In symmetrical 250 mM KCl, wild-type RyR1 had a mean conductance of ~800 pS (Fig. 3, Table 2). Removal of the negative charge in RyR1-$D^{4938}N$ (Fig. 4) significantly decreased K^+ conductance to 520 ± 6 pS (Table 2). The K^+ conductance of $D^{4945}N$ decreased to a lesser extent to 737 ± 11 pS (Table 2). RyR1-$E^{4952}Q$ (not shown) and RyR1-$E^{4955}Q$ (Table 2) showed a K^+ conductance not significantly different from wild-type. We conclude that the negatively charged side chain of D^{4938} (and to a lesser extent D^{4945}) influences K^+ permeation of RyR1.

TABLE 1 Ca^{2+}-release and [^{3}H]ryanodine-binding properties of wild-type and mutant RyR1s

Name	Caffeine-induced Ca^{2+} release	[^{3}H]Ryanodine binding
Vector	–	–
Wild-type RyR1	+++	+++
$D^{4938}N$	+++	+++
$E^{4942}Q$	–	–
$D^{4945}N$	+++	+++
$E^{4948}Q$	+++	+
$E^{4952}Q$	+++	+++
$D^{4953}N$	–	–
$E^{4955}Q$	+++	+++

(+++) indicates caffeine-induced Ca^{2+} release and [^{3}H]ryanodine binding activities comparable to wild-type RyR1; (+) indicates reduced activity; and (–) indicates no activity.

Cation selectivity of RyR1 mutants

RyRs permeate Ca^{2+} with a higher selectivity than K^+ (4–6). To determine the ion selectivity of the RyR1 mutants, current-voltage curves were recorded in 250 mM symmetric KCl with and without 10 mM Ca^{2+} in the *trans* (SR lumenal) bilayer chamber. The single channel currents and current-voltage relationships of wild-type (*solid symbols*) and RyR1-$D^{4938}N$ (*open symbols*) are compared (see Fig. 6 *A*) in the presence (*squares*) and absence (*circles*) of 10 mM *trans* Ca^{2+}. In the absence of Ca^{2+}, the K^+ currents showed linear voltage dependence. Addition of 10 mM Ca^{2+} to the *trans* chamber reduced currents at elevated positive and negative potentials. At 0 mV, a Ca^{2+} current of −2.8 pA for wild-type RyR1 and reduced current of −0.8 pA for $D^{4938}N$ were measured (Table 2). With the addition of Ca^{2+}, the reversal potentials (E_{rev}) for wild-type and $D^{4938}N$ were shifted to +9.5 and +5.3 mV, respectively, which gave permeability ratios of Ca^{2+}/K^+ (P_{Ca}/P_K) of 7.0 and 3.3. By comparison, RyR1-$D^{4945}N$ and $E^{4955}Q$ (Table 2) and $E^{4952}Q$ (not shown) had E_{rev} and P_{Ca}/P_K values not substantially different from wild-type.

Location of RyR1 mutants

The lumenal or cytosolic location of the RyR1 mutants, in relation to the selectivity filter, was assessed using neomycin. This large polycation has been shown to induce a voltage-dependent block in the open state of the cardiac ryanodine receptor (RyR2) from both ends of the channel (9–11). We examined the blocking effects of neomycin on wild-type and the two mutants that exhibited a reduced K^+ conductance (RyR1-$D^{4938}N$, -$D^{4945}N$) as well as one mutant (RyR1-$E^{4955}Q$) that had ion permeation not significantly different from wild-type. We also tested RyR1-$D^{4899}Q$ and -$E^{4900}N$, which are located on the lumenal loop of RyR1 (Fig. 1 *A*) and exhibit a reduced K^+ conductance and Ca^{2+} selectivity (Table 2).

To facilitate detection of neomycin-blocking events, wild-type RyR1 and mutant ion channels were modified using the neutral plant alkaloid ryanodine. Ryanodine forms in single channel recordings a subconductance (30) that is largely

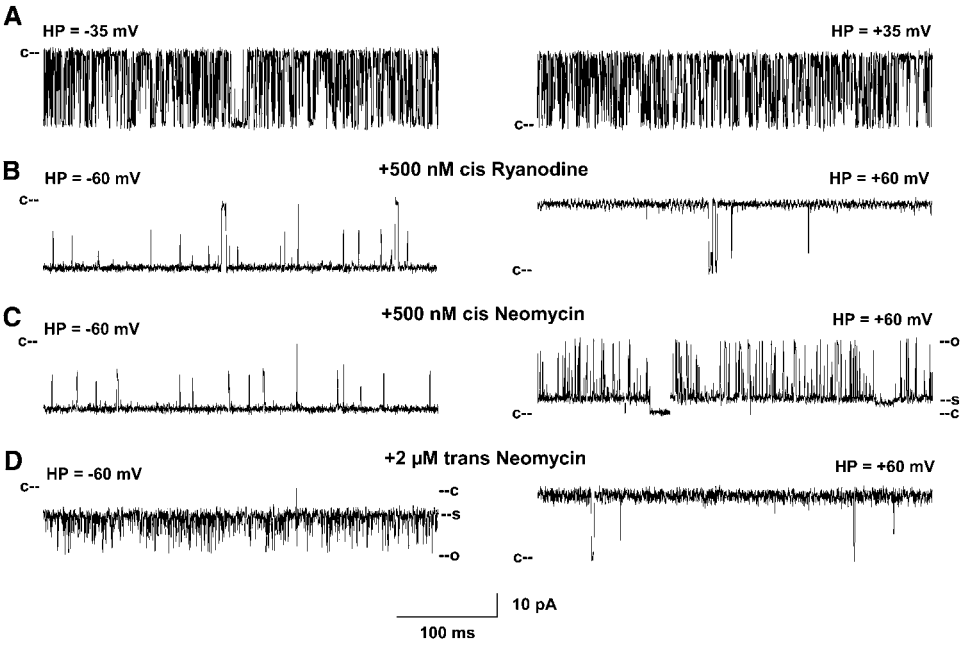

FIGURE 3 Single channel recordings of wild-type RyR1. (*A*) Single channel currents were recorded at indicated holding potentials in symmetrical 250 mM KCl with 2–20 μM Ca^{2+} and 1 mM ATP in the *cis* chamber as downward (*left*) or upward (*right*) inflections from the closed state (*c*–). (*B–D*) After addition of 500 nM ryanodine (*B*) and in subsequent presence of 500 nM *cis* (*C*) or 2 μM *trans* neomycin (*D*). In *C* and *D*, *c* and *o* represent the open and closed ryanodine-modified states; s represents the neomycin-induced substate.

insensitive to regulation by Ca^{2+} and ATP and other effectors. Moreover, neomycin does not permeate the ryanodine-modified RyR (10). Figs. 3–5 show that addition of ryanodine resulted in the formation of similarly prolonged channel openings in wild-type, $D^{4938}N$, and $D^{4899}Q$ single channels. Ryanodine induced subconductances in wild-type and mutant channels, corresponding to ~60% of the respective full conductances, with the exception of RyR1-$D^{4938}N$, which formed a subconductance corresponding to 75% of its full conductance (Table 2).

Neomycin induced a partial, voltage-dependent block in both ryanodine-modified wild-type RyR1 and mutants. When added to the *cis* (cytosolic) chamber of the bilayer apparatus, block was observed in wild-type at positive holding potentials (Fig. 3 and Fig. 6 *B*). The probability of the partial block (P_s) increased with neomycin concentration (Fig. 7 *A*). No blocking events were observed at negative holding potentials. Neomycin was considerably less effective in blocking RyR1-$D^{4938}N$ from the *cis* side at positive holding potentials (Figs. 4 and 7 *A*). When added to the *trans*

TABLE 2 Single channel properties of wild-type and mutant RyR1s

Parameter	wild-type	$D^{4899}Q$	$E^{4900}N$	$D^{4938}N$	$D^{4945}N$	$E^{4955}Q$
γ_{K+} (pS)	801 ± 7(17)†	164 ± 4(10)†*	505 ± 3(3)†*	520 ± 6(9)*	737 ± 11(6)*	812 ± 7(4)
$I_{Ca^{2+}}$ at 0 mV (pA)	−2.8 ± 0.1(7)†	−0.4 ± 0.1(4)†*	−2.0 ± 0.2(7)†*	−0.8 ± 0.1(4)*	−2.0 ± 0.2(5)*	−2.7 ± 0.2(3)
*E*rev (mV)	9.5 ± 0.2(6)†	1.9 ± 0.1(4)†*	6.8 ± 0.4(5)†*	5.3 ± 0.3(4)*	9.0 ± 0.6(5)	10.7 ± 0.7(3)
P_{Ca}/P_K	7.0†	1.0†	4.5†	3.3	6.5	8.3
$\gamma_{K+(+Ry)}$ (pS)	467 ± 19(8)	105 ± 2(9)*	296 ± 4(9)*	378 ± 8(6)*	429 ± 7(9)	457 ± 5(4)
$\gamma_{K+(+Ry)}/\gamma_{K+(-Ry)}$	0.58	0.62	0.59	0.75*	0.60	0.56
			+ *cis* Neomycin at 70 mV			
$\gamma_{sub(+Ry,+Neo)}/\gamma_{K+(+Ry)}$	0.16 ± 0.01(10)	0.37 ± 0.04(6)*	0.23 ± 0.01(8)*	0.49 ± 0.04(3)*	0.47 ± 0.01(3)*	0.15 ± 0.02 (3)
$k'_{on}(\mu M^{-1}\ ms^{-1})$	5.2 ± 0.8(7)	3.2 ± 0.7(3)	2.7 ± 0.3(3)	0.1 ± 0.1(3)*	2.2 ± 0.2(4)*	3.5 ± 0.3(3)
k_{off} (ms^{-1})	0.5 ± 0.1(6)	1.4 ± 0.1(3)*	0.5 ± 0.1(3)	0.8 ± 0.1(3)*	2.1 ± 0.1(4)*	0.3 ± 0.1(3)
K_{50} (μM)	0.1	0.5	0.2	11.1	0.9	0.1
Z_{total}	1.1 ± 0.1(10)	1.0 ± 0.1(3)	1.0 ± 0.1(3)	0.4 ± 0.1(3)*	1.2 ± 0.1(4)	1.1 ± 0.1(7)
			+*trans* Neomycin at −60 mV			
$\gamma_{sub(+Ry,+Neo)}/\gamma_{K+(+Ry)}$	0.39 ± 0.01(8)	‡	‡	0.50 ± 0.01(4)*	0.38 ± 0.01(4)	0.41 ± 0.01(6)
$k'_{on}(\mu M^{-1}\ ms^{-1})$	1.6 ± 0.2(5)	‡	‡	0.7 ± 0.2(4)*	0.6 ± 0.2(4)*	0.7 ± 0.1(5)*
k_{off} (ms^{-1})	1.4 ± 0.4(5)	‡	‡	2.3 ± 0.2(4)*	2.3 ± 0.2(4)*	2.1 ± 0.1 (5)*
K_{50} (μM)	0.8	‡	‡	3.5	3.1	2.4
Z_{total}	−0.6 ± 0.1(4)	‡	‡	−0.7 ± 0.1(4)	−0.6 ± 0.1(4)	−0.6 ± 0.1(7)

*$p < 0.05$ compared to wild-type.
†From Wang et al. (21).
‡Substate was not detected.
k_{off} was determined at 0.1 μM *cis* and 0.5 μM *trans* neomycin.

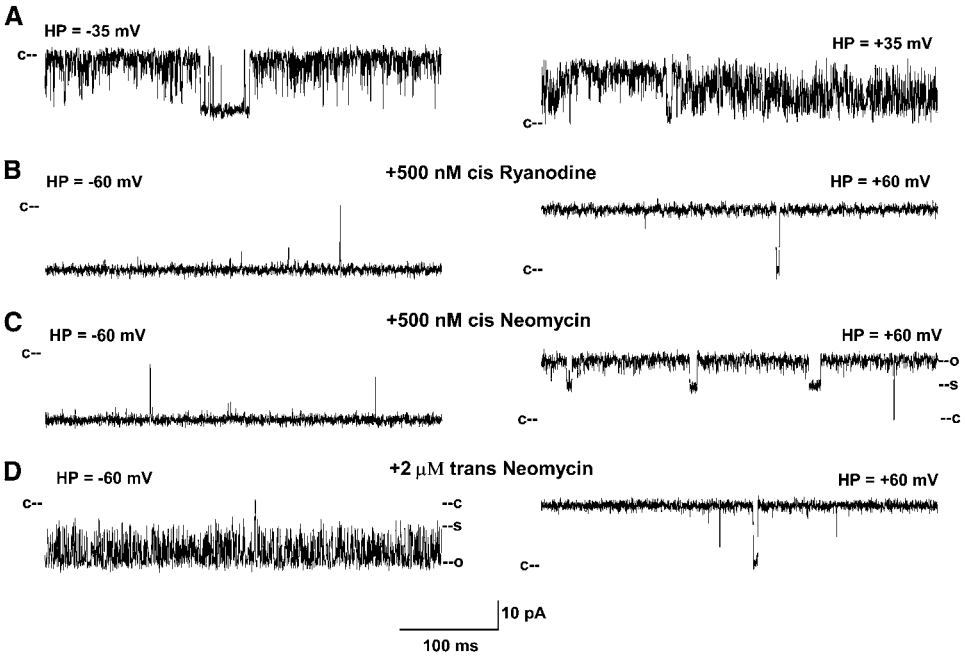

FIGURE 4 Single channel recordings of RyR1-D^{4938}N. (*A*) Single channel currents were recorded at indicated holding potentials in symmetrical 250 mM KCl with 2–20 μM Ca^{2+} and 1 mM ATP in the *cis* chamber as downward (*left*) or upward (*right*) inflections from the closed state (*c*–). (*B–D*) After addition of 500 nM ryanodine (*B*) and in subsequent presence of 500 nM *cis* (*C*) or 2 μM *trans* neomycin (*D*).

(SR lumenal) chamber, neomycin blocked wild-type RyR1 and D^{4938}N at negative but not positive holding potentials (Figs. 3 and 4, and Fig. 6 *B*).

The opposite results were obtained for RyR1-D^{4899}Q (Fig. 5). Neomycin induced a partial concentration- and voltage-dependent block from the cytosolic side, but failed to do so from the SR lumenal side. Voltage dependence of neomycin blocks on wild-type and mutant channels are summarized in Table 2. The results indicate that D^{4938} and D^{4945} are located in the cytosolic vestibule of RyR1. They further confirm that the negatively charged amino acid residues D^{4899} and E^{4900} are located on the lumenal side of the selectivity filter.

Kinetics of neomycin interaction with ryanodine-modified RyR1 mutant channels

The interactions of neomycin with the ryanodine-modified RyR channels were analyzed by determining the concentration dependence of the probability of substate occurrence (P_s). The dependence of P_s on the concentration of *cis* neomycin at +70 mV and *trans* neomycin at a holding potential of −60 mV is shown for wild-type RyR1 and D^{4938}N in Fig. 7 *A*. The data were fit with Eq. 2 and for wild-type yielded an apparent K_{50} of 0.1 and 0.8 μM for *cis* and *trans* neomycin, respectively (Table 2).

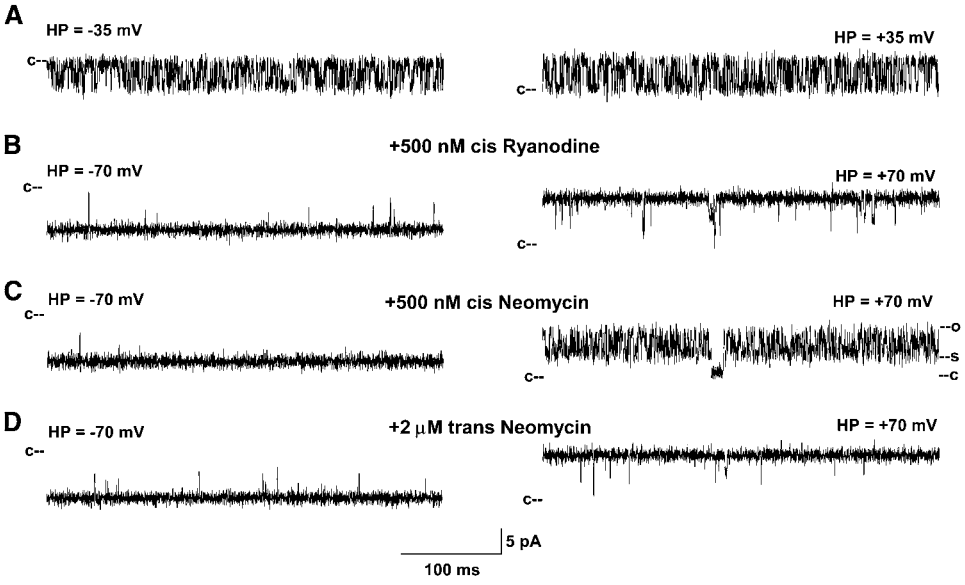

FIGURE 5 Single channel recordings of RyR1-D^{4899}Q. (*A*) Single channel currents were recorded at indicated holding potentials in symmetrical 250 mM KCl with 2–20 μM Ca^{2+} and 1 mM ATP in the *cis* chamber as downward (*left*) or upward (*right*) inflections from the closed state (*c*–). (*B–D*) After addition of 500 nM ryanodine (*B*) and in subsequent presence of 500 nM *cis* (*C*) or 2 μM *trans* neomycin (*D*).

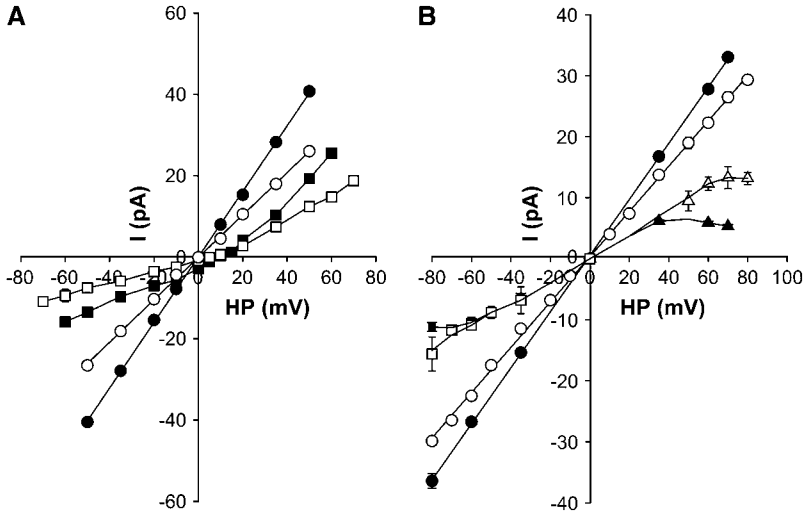

FIGURE 6 Current-voltage relationships of wild-type RyR1 and RyR1-$D^{4938}N$. (*A*) Representative current voltage relationships in 250 mM symmetrical KCl (●, wild-type; ○, $D^{4938}N$) and with the subsequent addition of 10 mM *trans* Ca^{2+} (■, wild-type; □, $D^{4938}N$). (*B*) Representative current voltage relationships in 250 mM symmetrical KCl of ryanodine-modified channels (●, wild-type; ○, $D^{4938}N$) and substate current voltage relationships after the subsequent addition of 500 nM *cis* (▲, wild-type; Δ, $D^{4938}N$) or *trans* (■, wild-type; □, $D^{4938}N$) neomycin. Note, not shown is the absence of *cis* and *trans* neomycin block at negative and positive holding potentials, respectively.

Removal of negative charges from D^{4938} attenuated neomycin block to a greater extent from the *cis* than from the *trans* side. For $D^{4938}N$, the averaged K_{50} of *cis* neomycin block was increased by >100-fold compared to wild-type. A ninefold increase in K_{50} of *cis* neomycin block was calculated for $D^{4945}N$ (Table 2). No changes in apparent affinity of neomycin block from the *cis* side were observed for RyR1-$E^{4955}Q$. In comparison, charge neutralization of RyR1-D^{4899} and -E^{4900} predominantly affected neomycin block from the *trans* side. A blocking action of neomycin from the *trans* side was not observed for $D^{4899}Q$ and $E^{4900}N$. Interestingly, charge neutralization also affected K_{50} of neomycin block of $D^{4938}N$, $D^{4945}N$, and $E^{4955}Q$ from the *trans* side and block of $D^{4899}Q$ and $E^{4900}N$ from the *cis* side (Table 2).

We also determined the voltage and concentration dependence of association and dissociation rates of neomycin block. Consistent with the above data, the on rate of *cis* neomycin block increased linearly as a function of neomycin concentration at +70 mV, yielding an association rate constant (k'_{on}) of 5.2 $s^{-1}\mu M^{-1}$ for wild-type and a greatly reduced association rate constant of 0.1 $s^{-1}\mu M^{-1}$ for $D^{4938}N$ (Fig. 7 *B*, Table 2).

The dissociation rates of neomycin decreased as the concentration of neomycin in the *cis* and *trans* chambers was increased to 1 μM (0.5 μM for wild-type) and 2 μM,

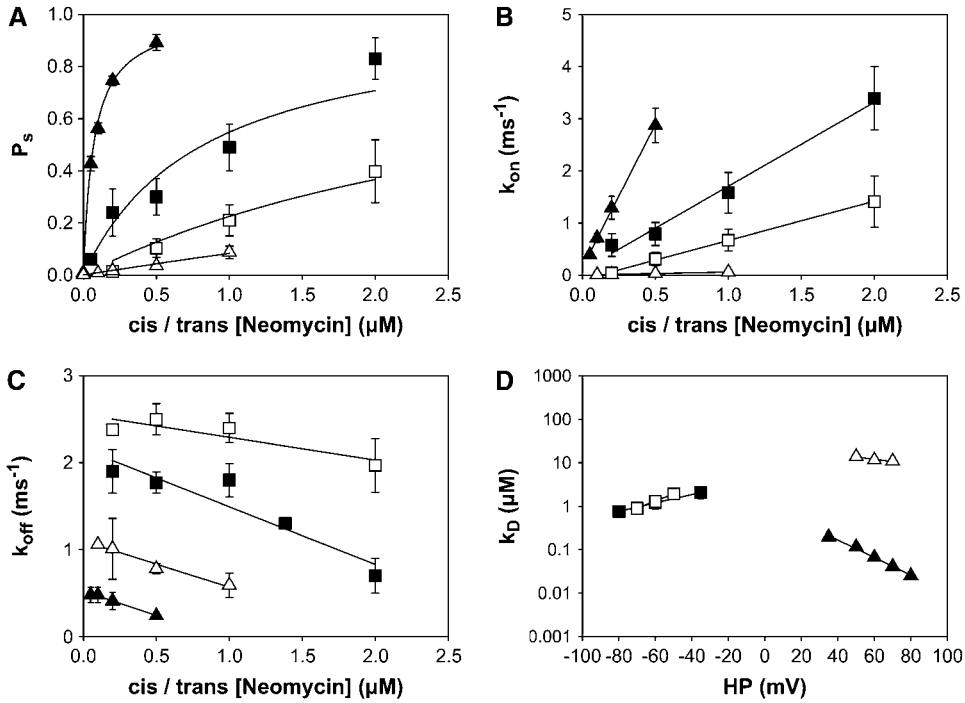

FIGURE 7 Kinetic parameters of neomycin block on wild-type RyR1 and RyR1-$D^{4938}N$. (*A*) P_s dependence of wild-type and $D^{4938}N$ on *cis* (at +70 mV) and *trans* (at −60 mV) neomycin concentration. The lines represent the fits to the data using Eq. 2. (*B* and *C*) Dependence of association (*B*) and dissociation (*C*) rates of wild-type and $D^{4938}N$ on *cis* (at +70 mV) and *trans* (at −60 mV) neomycin concentration. k_{on} and k_{off} were obtained using Eqs. 3 and 4. (*D*) Relationship between K_D and holding potential of *cis* and *trans* neomycin block on wild-type and $D^{4938}N$. Neomycin concentrations were 0.5 μM for wild-type and 1 μM for $D^{4938}N$. Lines represent the fits obtained using Eq. 6. (*A–D*) *cis* neomycin (▲, wild-type; Δ, $D^{4938}N$) and *trans* neomycin (■, wild-type; □, $D^{4938}N$). Data were obtained from recordings similar to those shown for wild-type in Fig. 3, *C* and *D*, and for $D^{4938}N$ in Fig. 4, *C* and *D*. Each point represents the mean ± SE of 4–7 experiments.

respectively (Fig. 7 *C*). The reasons for these decreases are unclear. Dependence of k_{off} on neomycin concentration was also observed for the native cardiac RyR2 (9). In contrast, ryanodine-modified RyR2 channels did not show neomycin dependence at low concentrations (0–200 nM) (10). In this study, k_{off} in Table 2 was determined at 0.1 μM *cis* and 0.5 μM *trans* neomycin, i.e., where k_{off} was largely independent on neomycin concentration (Fig. 7 *C*). The ratio of the rate constants, k_{off}/k_{on}', for wild-type and $D^{4938}N$ in the presence of *cis* neomycin yielded K_D of 0.1 and 8 μM. Respective ratios in the presence of *trans* neomycin were 0.9 and 3.3. The four ratios were in reasonable agreement with dissociation equilibrium constants (K_{50}) obtained using probability function curves of substate occurrence (P_s).

The voltage dependence of the rate constants was analyzed by the Boltzmann equation (Eq. 6). As shown in Fig. 7 *D*, K_D of *cis* neomycin block on wild-type RyR1 and $D^{4938}N$ decreased as the holding potential was made more positive. K_D of *trans* neomycin block decreased as the holding potential became more negative. The solid lines drawn through the points were obtained by linear regression, and the values of total effective gating charges (z_{total}) obtained from the slopes of these lines for *cis* neomycin were 1.1 for wild-type and 0.4 for $D^{4938}N$. Similar z_{total} values were obtained for *trans* neomycin (-0.6 and -0.7 for wild-type and $D^{4938}N$, respectively).

The kinetic parameters of neomycin block from the *cis* and *trans* sides for wild-type and mutants are summarized in Table 2. For $D^{4938}N$, an ~50-fold decrease in the association rate constant was primarily responsible for the reduced affinity of neomycin binding from the *cis* side. z_{total} was 0.4 compared to 1.1 for wild-type, suggesting a change in the location of the neomycin binding site and/or the voltage drop when the charge on D^{4938} is neutralized. For $D^{4945}N$, a 2.4-fold decrease in k_{on} and a 4-fold increase in k_{off} yielded a nearly 10-fold increase in the equilibrium dissociation constant compared to wild-type without a change in z_{total}. Significant differences in the rate constants were also calculated for $D^{4938}N$, $D^{4945}N$, and $E^{4955}Q$ from the *trans* side and for $D^{4899}Q$ from the *cis* side. However, these differed by <3-fold compared to wild-type. Collectively, the data are consistent with the notion that neomycin blocks the skeletal muscle RyR by binding with high affinity to cytosolic (D^{4938}) and lumenal (D^{4899}, E^{4900}) pore sites.

DISCUSSION

This study identified by mutagenesis negatively charged residues that affect K^+ ion permeation (D^{4938}, D^{4945}) and Ca^{2+} ion selectivity (D^{4938}). No changes in K^+ ion permeation and Ca^{2+} selectivity were observed for two other RyR1 mutants ($E^{4952}Q$, $E^{4955}Q$). These four mutants ($D^{4938}N$, $D^{4945}N$, $E^{4952}Q$, $E^{4955}Q$) maintained caffeine-induced Ca^{2+} release, [^{3}H]ryanodine binding, and regulation by Ca^{2+} in [^{3}H]ryanodine binding and single channel measurements, indicating no major alterations in protein structure. In a previous study, we showed that two conserved negatively charged amino acid residues (D^{4899}, E^{4900}) immediately after the selectivity filter motif GGGIG play a critical role in RyR1 ion permeation and selectivity (21). Charge neutralization of D^{4899}, and to a lesser extent of E^{4900}, reduced K^+ ion conductance and selectivity for Ca^{2+} compared to K^+.

We further showed that charge neutralization of D^{4938} (and to a lesser extent D^{4945}) attenuated the block of neomycin from the cytosolic side, whereas charge neutralization of D^{4899} and E^{4900} removed the block from the lumenal side. The results suggest the presence of rings of negative charges in the lumenal (D^{4899} and E^{4900}) and cytosolic (D^{4938} and D^{4945}) vestibules that are required for maintaining the high rates of RyR1 ion fluxes. They further suggest that the lumenal D^{4899} and E^{4900} and cytosolic D^{4938} loci represent major cation-blocking sites in the tetrameric RyRs.

Previous studies have indicated that mutations in the final membrane domain affect RyR channel function. Naturally occurring mutations that give rise to two skeletal muscle-associated diseases, malignant hyperthermia and central core disease, are clustered in three regions of RyR1, one of which is the pore-forming region of RyR1 (31). A RyR1-G^{4941} mutation was detected in a patient whose muscle biopsy exhibited a sustained increase in muscle tension at a low halothane concentration (32). In another patient, deletion of two amino acid residues (V^{4926}, I^{4927}) caused central core disease (33). The deletion abolished [^{3}H]ryanodine binding and Ca^{2+} responsiveness, and in single channel measurements exhibited a reduced K^+ conductance and Ca^{2+} selectivity, indicating major alterations in protein conformation and pore structure (34). Wang et al. (35,36) used alanine and glycine scanning mutagenesis to show that the final membrane domain is an important determinant of [^{3}H]ryanodine binding and channel activity. In another study, two RyR1-D^{4938} mutants ($D^{4938}N$, $D^{4938}E$) maintained caffeine-induced Ca^{2+} release and [^{3}H]ryanodine binding (37). This work extends the above studies by showing that mutagenesis of RyR1-D^{4938} and D^{4945} to asparagine modified RyR1 ion fluxes.

We used the large polycation neomycin to probe the location of negatively charged amino acid residues. In agreement with previous single channel measurements of the cardiac ryanodine receptor (9–11), neomycin induced partial blocking events when added to the lumenal or cytosolic side of wild-type RyR1. To facilitate analysis of interaction of neomycin with our mutant channels, experiments were performed using ryanodine-modified channels. For all mutants, differences in blocking parameters were observed. The most significant effect of removing a negative charge was observed for $D^{4899}Q$ and $E^{4900}N$, as addition of neomycin to the *trans* chamber failed to produce noticeable blocking events in the two mutant channels. Removal of negative charge from D^{4938} had a less severe effect. It greatly attenuated, but did not eliminate, neomycin block from the cytosolic side.

Charge neutralization primarily affected the blocking potency of *cis* neomycin by decreasing the on rate of neomycin binding to $D^{4938}N$. The results suggest a lessening of attractive charge interactions between the polycation neomycin and channel regions of high negative charge density. Because of the proximity of four negative charges in the homotetrameric RyR, such regions are expected to be formed on the lumenal (D^{4899} and E^{4900}) and cytosolic (D^{4938}) sides of the selectivity filter. Interestingly, charge neutralization of lumenal D^{4899} influenced the magnitude and affinity of neomycin block from the *cis* side, and vice versa the cytosolic mutants $D^{4938}N$, $D^{4945}N$, and $E^{4955}Q$ affected neomycin block from the lumenal side. The reason for this is unclear. One possibility we cannot rule out is that these mutations modified the structure of the pore.

Mutagenesis also resulted in a change of the voltage dependence of neomycin block in one mutant ($D^{4938}N$). Total effective gating charges (z_{total}) of wild-type RyR1 for cytosolic and lumenal neomycin were 1.1 and −0.6, respectively. Dividing these numbers by the nominally four positive charges of neomycin yields an electrical distance of 0.27 from the cytosolic side and 0.15 from the lumenal side for the location of the neomycin binding sites in the voltage drop of wild-type RyR1. However, these distances may be substantially underestimated because it is not known how many of the positive charges of neomycin interact with the voltage drop. z_{total} values comparable to wild-type indicate a similar relative location of cytosolic- and lumenal neomycin-blocking sites in wild-type and mutant channels. One exception was RyR1-$D^{4938}N$ where a 2–3-fold reduction in z_{total} for *cis* neomycin suggests a major change in the relative location of the neomycin-blocking site, voltage drop, or both.

One model of the RyR pore structure that is consistent with our results is shown in Fig. 8. The model is based on the known structure of the K^+ channels (26) and is in good agreement with two recent cryoelectron microscopy studies that determined the pore structure of the closed RyR1 ion channel at a resolution of 13.6 Å (38) and 9.6 Å (39), based on a Fourier shell cutoff criterion at 0.5. Both studies revealed a RyR1 pore structure similar to that of K^+ channels. Structural elements visualized in the RyR1 transmembrane domain at 13.6 Å resolution included a shallow lumenal vestibule, a constriction of the pore (the selectivity filter), an inner vestibule, four high-density rod-like structures that merged into a dense ring (termed ion gate), and a wide cytosolic vestibule (38). Ludtke et al. (39) resolved at the higher resolution five helices in the membrane-spanning region including a transmembrane helix and short helix both lining the pore. A kink in the transmembrane helix suggested the presence of a ''gating hinge'' glycine (G^{4934}) as observed in K^+ channels (26).

In the model shown in Fig. 8, we introduced a break near RyR1-D^{4938} in the helical structure of the putative inner helix of the RyR1 ion pore, based on secondary structure predictions. RyR1-D^{4938} is part of a conserved GLIIDAF motif

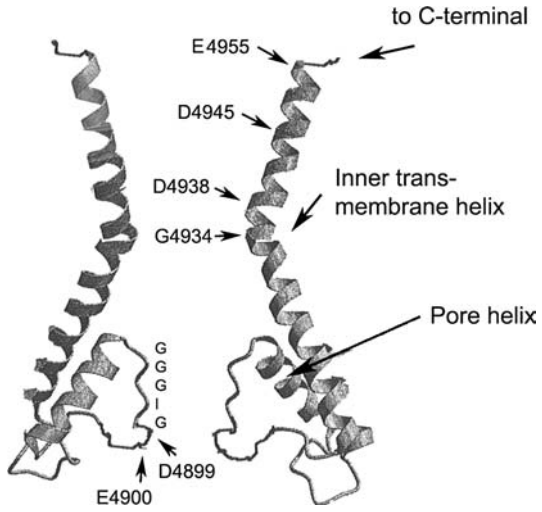

FIGURE 8 Hypothetical model for ion pore of RyR1. The RyR1 pore model, which was obtained by modifying by ''hand'' the published structure of K^+ channels (24,26), shows the putative position of lumenal amino acid residues D^{4899} and E^{4900} and cytosolic amino acid residues G^{4934}, D^{4938}, D^{4945}, and E^{4955}. The inner transmembrane helix in RyR1 is analogous to S6 in 6TM K^+ channels (such as *Shaker* and KvAP) and M2 in 2TM K^+ channels (such as KcsA and Kir). Note only two of the four pore-forming segments are shown.

in the RyRs and GVIIDTF motif in the related inositol receptors (IP_3Rs). Secondary structure predictions indicate a high helical probability for the putative inner helix and succeeding ~16 amino acid residues (Fig. 1 *C*). A decrease at RyR1-G^{4934} suggests a potential break in the helical structure of the inner helix and widening of the cytosolic vestibule, as has been found in K^+ channels (26). In K^+ channels, a ''gating hinge glycine'' residue bends the inner helix by ~30° and widens the cytosolic vestibule of the open channels. The presence of an enlarged RyR1 vestibule is consistent with our observation that acidic residues following RyR1-D^{4938} appear to have a lesser role in RyR1 ion permeation and selectivity. We also note that an extended cytosolic vestibule (38,39) can be expected to favor retention of neomycin in the conductance pathway at positive voltages and provides a likely explanation that neomycin blocks RyRs more effectively from the cytosolic than lumenal side ((11), this study).

Two models have been recently described to account for the ion fluxes through RyRs. Molecular dynamic simulations identified several kinetically important residues that slowed the velocity of K^+ and Ca^{2+} movement through the RyR2 pore (40). At variance with our experimental results ((21), this study), RyR2-D^{4831} (equivalent to RyR1-D^{4899}) and RyR2-D^{4870} (equivalent to RyR1-D^{4938}) were not identified as major kinetic barriers that reduced the rates of ion translocation.

In a model of ion permeation through RyR, we have shown that the effects of neutralizing the negatively charged carboxyl oxygens of RyR1-D^{4899} and -E^{4900} are well

reproduced by a Poisson-Nernst-Planck/Density Functional Theory (PNP/DFT) model that describes the electrodiffusion of finite-sized ions down their chemical potential gradients (41). Interestingly, the model suggests that, in addition to the negatively charged lumenal residues D^{4899} and E^{4900}, some negative charges in the cytosolic atrium are critical for maintaining high rates of RyR ion flux and selectivity. Whether D^{4938} and D^{4945} can account for the negative charges in the cytosolic vestibule predicted by the PNP/DFT model remains to be determined.

SUPPLEMENTARY MATERIAL

An online supplement to this article can be found by visiting BJ Online at http://www.biophysj.org.

The authors thank Daniel Pasek and Kelly Evans for purifying and determining the activities of the RyR1 mutants.

Support by National Institutes of Health Grant AR18687 is gratefully acknowledged.

REFERENCES

1. Fill, M., and J. A. Copello. 2002. Ryanodine receptor calcium release channels. *Physiol. Rev.* 82:893–922.
2. Franzini-Armstrong, C., and F. Protasi. 1997. Ryanodine receptors of striated muscles: a complex channel capable of multiple interactions. *Physiol. Rev.* 77:699–729.
3. Meissner, G. 2002. Regulation of mammalian ryanodine receptors. *Front. Biosci.* 7:d2072–d2080.
4. Liu, Q. Y., F. A. Lai, E. Rousseau, R. V. Jones, and G. Meissner. 1989. Multiple conductance states of the purified calcium release channel complex from skeletal sarcoplasmic reticulum. *Biophys. J.* 55:415–424.
5. Smith, J. S., T. Imagawa, J. Ma, M. Fill, K. P. Campbell, and R. Coronado. 1988. Purified ryanodine receptor from rabbit skeletal muscle is the calcium-release channel of sarcoplasmic reticulum. *J. Gen. Physiol.* 92:1–26.
6. Tinker, A., A. R. Lindsay, and A. J. Williams. 1992. A model for ionic conduction in the ryanodine receptor channel of sheep cardiac muscle sarcoplasmic reticulum. *J. Gen. Physiol.* 100:495–517.
7. Tinker, A., and A. J. Williams. 1993. Using large organic cations to probe the nature of ryanodine modification in the sheep cardiac sarcoplasmic reticulum calcium release channel. *Biophys. J.* 65:1678–1683.
8. Xu, L., R. Jones, and G. Meissner. 1993. Effects of local anesthetics on single channel behavior of skeletal muscle calcium release channel. *J. Gen. Physiol.* 101:207–233.
9. Mead, F., and A. J. Williams. 2002. Block of the ryanodine receptor channel by neomycin is relieved at high holding potentials. *Biophys. J.* 82:1953–1963.
10. Mead, F., and A. J. Williams. 2002. Ryanodine-induced structural alterations in the RyR channel suggested by neomycin block. *Biophys. J.* 82:1964–1974.
11. Mead, F. C., and A. J. Williams. 2004. Electrostatic mechanisms underlie neomycin block of the cardiac ryanodine receptor channel (RyR2). *Biophys. J.* 87:3814–3825.
12. Xu, L., A. Tripathy, D. A. Pasek, and G. Meissner. 1999. Ruthenium red modifies the cardiac and skeletal muscle Ca^{2+} release channels (ryanodine receptors) by multiple mechanisms. *J. Biol. Chem.* 274: 32680–32691.
13. Takeshima, H., S. Nishimura, T. Matsumoto, H. Ishida, K. Kangawa, N. Minamino, H. Matsuo, M. Ueda, M. Hanaoka, T. Hirose, and S. Numa. 1989. Primary structure and expression from complementary DNA of skeletal muscle ryanodine receptor. *Nature.* 339:439–445.
14. Zorzato, F., J. Fujii, K. Otsu, M. Phillips, N. M. Green, F. A. Lai, G. Meissner, and D. H. MacLennan. 1990. Molecular cloning of cDNA encoding human and rabbit forms of the Ca^{2+} release channel (ryanodine receptor) of skeletal muscle sarcoplasmic reticulum. *J. Biol. Chem.* 265:2244–2256.
15. Du, G. G., G. Avila, P. Sharma, V. K. Khanna, R. T. Dirksen, and D. H. MacLennan. 2004. Role of the sequence surrounding predicted transmembrane helix M4 in membrane association and function of the Ca^{2+} release channel of skeletal muscle sarcoplasmic reticulum (ryanodine receptor isoform 1). *J. Biol. Chem.* 279:37566–37574.
16. Wang, R., L. Zhang, J. Bolstad, N. Diao, C. Brown, L. Ruest, W. Welch, A. J. Williams, and S. R. Chen. 2003. Residue Gln4863 within a predicted transmembrane sequence of the Ca^{2+} release channel (ryanodine receptor) is critical for ryanodine interaction. *J. Biol. Chem.* 278:51557–51565.
17. Balshaw, D., L. Gao, and G. Meissner. 1999. Luminal loop of the ryanodine receptor: a pore-forming segment? *Proc. Natl. Acad. Sci. USA.* 96:3345–3347.
18. Chen, S. R., P. Li, M. Zhao, X. Li, and L. Zhang. 2002. Role of the proposed pore-forming segment of the Ca^{2+} release channel (ryanodine receptor) in ryanodine interaction. *Biophys. J.* 82:2436–2447.
19. Du, G. G., X. Guo, V. K. Khanna, and D. H. MacLennan. 2001. Functional characterization of mutants in the predicted pore region of the rabbit cardiac muscle Ca^{2+} release channel (ryanodine receptor isoform 2). *J. Biol. Chem.* 276:31760–31771.
20. Gao, L., D. Balshaw, L. Xu, A. Tripathy, C. Xin, and G. Meissner. 2000. Evidence for a role of the lumenal M3–M4 loop in skeletal muscle Ca^{2+} release channel (ryanodine receptor) activity and conductance. *Biophys. J.* 79:828–840.
21. Wang, Y., L. Xu, D. A. Pasek, D. Gillespie, and G. Meissner. 2005. Probing the role of negatively charged amino acid residues in ion permeation of skeletal muscle ryanodine receptor. *Biophys. J.* 89: 256–265.
22. Zhao, M., P. Li, X. Li, L. Zhang, R. J. Winkfein, and S. R. Chen. 1999. Molecular identification of the ryanodine receptor pore-forming segment. *J. Biol. Chem.* 274:25971–25974.
23. Grunwald, R., and G. Meissner. 1995. Lumenal sites and C terminus accessibility of the skeletal muscle calcium release channel (ryanodine receptor). *J. Biol. Chem.* 270:11338–11347.
24. Doyle, D. A., J. Morais Cabral, R. A. Pfuetzner, A. Kuo, J. M. Gulbis, S. L. Cohen, B. T. Chait, and R. MacKinnon. 1998. The structure of the potassium channel: molecular basis of K^+ conduction and selectivity. *Science.* 280:69–77.
25. Tinker, A., and A. J. Williams. 1993. Probing the structure of the conduction pathway of the sheep cardiac sarcoplasmic reticulum calcium-release channel with permeant and impermeant organic cations. *J. Gen. Physiol.* 102:1107–1129.
26. Jiang, Y., A. Lee, J. Chen, M. Cadene, B. T. Chalt, and R. MacKinnon. 2002. The open pore conformation of potassium channels. *Nature.* 417:523–526.
27. Sutko, J. L., J. A. Airey, W. Welch, and L. Ruest. 1997. The pharmacology of ryanodine and related compounds. *Pharmacol. Rev.* 49:53–98.
28. Xu, L., and G. Meissner. 1998. Regulation of cardiac muscle Ca^{2+} release channel by sarcoplasmic reticulum lumenal Ca^{2+}. *Biophys. J.* 75:2302–2312.
29. Schoenmakers, T. J., G. J. Visser, G. Flick, and A. P. R. Theuvenet. 1992. CHELATOR: an improved method for computing metal ion concentrations in physiological solutions. *Biotechniques.* 12:870–879.
30. Rousseau, E., J. S. Smith, and G. Meissner. 1987. Ryanodine modifies conductance and gating behavior of single Ca^{2+} release channel. *Am. J. Physiol.* 253:C364–C368.

31. Brini, M. 2004. Ryanodine receptor defects in muscle genetic diseases. *Biochem. Biophys. Res. Commun.* 322:1245–1255.

32. Galli, L., A. Orrico, S. Cozzolino, V. Pietrini, V. Tegazzin, and V. Sorrentino. 2002. Mutations in the RYR1 gene in Italian patients at risk for malignant hyperthermia: evidence for a cluster of novel mutations in the C-terminal region. *Cell Calcium.* 32:143–151.

33. Davis, M. R., E. Haan, H. Jungbluth, C. Sewry, K. North, F. Muntoni, T. Kuntzer, P. Lamont, A. Bankier, P. Tomlinson, A. Sanchez, P. Walsh, L. Nagarajan, C. Oley, A. Colley, A. Gedeon, R. Quinlivan, J. Dixon, D. James, C. R. Muller, and N. G. Laing. 2003. Principal mutation hotspot for central core disease and related myopathies in the C-terminal transmembrane region of the RYR1 gene. *Neuromuscul. Disord.* 13:151–157.

34. Lyfenko, A. D., S. Ducreux, Y. Wang, L. Xu, F. Zorzato, A. Ferreiro, G. Meissner, S. Treves, and R. T. Dirksen. 2005. Two central core disease (CCD) deletions in the C-terminal region of RyR1 alter muscle EC coupling by distinct mechanisms. *Biophys. J.* 88:488a. (Abstr.)

35. Wang, R., J. Bolstad, H. *Kong*, L. Zhang, C. Brown, and S. R. W. Chen. 2004. The predicted TM10 transmembrane sequence of the cardiac Ca^{2+} release channel (ryanodine receptor) is crucial for channel activation and gating. *J. Biol. Chem.* 279:3635–3642.

36. Wang, R., L. Zhang, J. Bolstad, N. Diao, C. Brown, L. Ruest, W. Welch, A. J. Williams, and S. R. W. Chen. 2003. Residue Gln^{4863} within a predicted transmembrane sequence of the Ca^{2+} release channel (ryanodine receptor) is critical for ryanodine interaction. *J. Biol. Chem.* 278:51557–51565.

37. Du, G. G., and D. H. MacLennan. 1998. Functional consequences of mutations of conserved, polar amino acids in transmembrane sequences of the Ca^{2+} release channel (ryanodine receptor) of rabbit skeletal muscle sarcoplasmic reticulum. *J. Biol. Chem.* 273:31867–31872.

38. Samso, M., T. Wagenknecht, and P. D. Allen. 2005. Internal structure and visualization of transmembrane domains of RyR1 calcium release channel by cryo-EM. *Nat. Struct. Mol. Biol.* 12:539–544.

39. Ludtke, S. J., I. I. Serysheva, S. L. Hamilton, and W. Chiu. 2005. The pore structure of the closed RyR1 channel. *Structure.* 13: 1203–1211.

40. Welch, W., S. Rheault, D. J. West, and A. J. Williams. 2004. A model of the putative pore region of the cardiac ryanodine receptor channel. *Biophys. J.* 87:2335–2351.

41. Gillespie, D., L. Xu, Y. Wang, and G. Meissner. 2005. (De)constructing the ryanodine receptor: modeling ion permeation and selectivity of the calcium release channel. *J. Phys. Chem. B.* 109:15598–15610.

42. Rost, B., P. Fariselli, and R. Casadio. 1996. Topology prediction for helical transmembrane proteins at 86% accuracy. *Protein Sci.* 7:1704–1718.

43. Rost, B., and C. Sander. 1993. Prediction of protein secondary structure at better than 70% accuracy. *J. Mol. Biol.* 232:584–599.